GPS Solutions (2021) 25:144
https://doi.org/10.1007/s10291-021-01179-y

ORIGINAL ARTICLE

Code and phase multipath mitigation by using the observation-domain parameterization and its application in five-frequency GNSS ambiguity resolution

Zhetao Zhang[1]

Received: 10 January 2021 / Accepted: 11 September 2021 / Published online: 25 September 2021

Abstract
In multi-frequency and multi-constellation GNSS applications, the multi-frequency carrier ambiguity resolution (MCAR) is the prerequisite of high-precision positioning and navigation. Since the multipath is the main unmodeled error that cannot be easily mitigated, we first propose a new code and phase multipath mitigation method using a way of observation-domain parameterization, which can be applied to the GNSS like MCAR, including four-frequency and five-frequency carrier ambiguity resolution (FiCAR). First, take the five-frequency BDS-3 data as an example; the necessity of multipath mitigation in linear combinations is discussed. Second, for the proposed method, the between-receiver single-differenced (SD) multi-frequency multipath combinations are formed and preprocessed. Then the SD multipath can be estimated by the least squares. Finally, the multipath-reduced observations can be applied to the MCAR. Real five-frequency observations with multipath are tested. The proposed method is compared with the traditional method ignoring the multipath by using the single-epoch and multi-epoch modes, including the geometry-free and geometry-based models. The results indicate that the success rate and efficiency of ambiguity resolution can be improved significantly. Specifically, in the single-epoch mode, only the ambiguity resolution success rates of the proposed method are all 100% for the first to fourth signals. Besides, when fixing the fifth signal, the improvement of ambiguity resolution success rates can reach 19.4% on average. For the first four signals in the multi-epoch mode, the mean time-to-first-fix values of the traditional and improved methods are 18.25 and 1.00 s, respectively, and approximately 49 s can be shortened for the fifth signal. Undifferenced or double-differenced multipath can also be parameterized similarly, and then be used in other real-time or kinematic GNSS applications.

Keywords Multi-frequency GNSS · Code and phase multipath · Multipath mitigation · Observation-domain parameterization · Ambiguity resolution

Introduction

With the opening of the five-frequency BDS-3 system, the technology of multi-frequency and multi-constellation conditions is the general trend in GNSS applications. The ambiguity resolution (AR) is the prerequisite of high-precision positioning and navigation, such as real-time kinematic positioning (RTK). In order to improve the success rate and efficiency of AR, the error terms of code and phase observations should be processed appropriately. However, unmodeled errors such as atmospheric delays and multipath usually cannot be ignored (Li et al. 2018).

Earlier research mainly focuses on obtaining the ambiguities with high efficiency and high reliability by using single-frequency or dual-frequency data. The criterion is systematically studied, including rounding, bootstrapping, or integer least-squares (ILS) criterion (Dong and Bock 1989; Teunissen 1993, 1998). The rounding strategy is simple, but the correlations of float ambiguities are ignored, and the bootstrapping method only takes the correlations between adjacent ambiguities into account. The ILS criterion then accounts for all the correlations by finding the minimum norm fixed solutions according to the covariance matrix of the ambiguities (Teunissen et al. 2002). The decorrelation method is then used in ILS (Teunissen 1995). Later, the emergence of three-frequency GNSS brings great benefits

✉ Zhetao Zhang
ztzhang@hhu.edu.cn

[1] School of Earth Sciences and Engineering, Hohai University, Nanjing 211100, China

to AR. Forssell et al. (1997) and Vollath et al. (1998) proposed the concept of three-frequency carrier ambiguity resolution (TCAR). Typically, the TCAR method means that the ambiguities of the selected linear phase combinations are fixed by rounding directly according to a certain order. The success rate and efficiency of AR are improved significantly by the TCAR method (Cocard et al. 2008). As usual, the TCAR method is based on the geometry-free (GF) model. The geometry-based (GB) model which has better geometric strength, can also be used (Feng 2008; Zhang and He 2016). More recently, since the BDS-3 and Galileo satellites can broadcast four or five frequencies, four-frequency carrier ambiguity resolution (FCAR) or five-frequency carrier ambiguity (FiCAR) became possible, improving the success rate and efficiency of AR even further (Zhang et al. 2020).

In multi-frequency carrier ambiguity resolution (MCAR), including TCAR, FCAR, and FiCAR, mitigating or even avoiding the impacts of unmodeled errors is one of the most important issues since it will deteriorate the accuracy of float ambiguities. The tropospheric and ionospheric delays can be largely eliminated or mitigated via observation combination, model correction, or parameterization (Wang and Rothacher 2013; Li 2018). Li et al. (2010) proposed a distance-independent AR method using a GF and ionospheric-free (IF) semi-generated signal. Zhao et al. (2015) applied a modified TCAR method to mitigate the residual ionospheric delays in three-frequency linear combinations. Since the BDS system has three types of satellites, the BDS-2 or BDS-3 AR is also investigated (Tang et al. 2014; Li et al. 2020). Because multipath cannot be treated by the above traditional methods (Luo et al. 2014; Leick et al. 2015; Zhang et al. 2019), using additional data processing methods is an indispensable approach, especially in canyon environment, low-cost receiver, and long baseline. As usual, the signals with longer wavelengths are more affected by multipath (Lima Filho and Moraes 2020). Based on the satellite period, the sidereal filtering is used, where the undifferenced (UD), single-differenced (SD), or double-differenced (DD) strategy in either the coordinate (Bock et al. 2000; Ragheb et al. 2007) or observation (Zhong et al. 2010; Ye et al. 2015) domain can be conducted. Thanks to the spatial repeatability of satellites, in a static or relative static condition, a so-called hemispherical map providing multipath corrections can also be applied (Moore et al. 2014; Fuhrmann et al. 2015); for the relative and standalone modes, see Dong et al. (2016) and Zheng et al. (2019) respectively. In addition, the other strategies can also be applied, such as the front-end signal processing (McGraw and Braasch 1999; Henkel et al. 2016), advanced tracking method (Yang et al. 2020), improved antenna array (Daneshmand et al. 2013), wavelet analysis (Pugliano et al. 2016), ray-tracing method (Lau and Cross 2007), support vector regression (Phan et al. 2013), and Vondrak filtering (Zheng et al. 2005).

However, currently, there are still some limitations of multipath processing, of course including in the area of MCAR. First, as aforementioned, the traditional multipath processing methods mainly focus on the non-parametric way, where the errors cannot be fully captured or eliminated. Limited research focuses on multipath mitigation in the MCAR (Moradi et al. 2015; Chen et al. 2016; Wang et al. 2018). This topic is crucial since the multipath effects are amplified in the MCAR, which will be proved in the following text. In essence, most of these methods are like the model correction in the time or space field. At present, there is no universal observation-domain parameterized method for code and phase observations. In theory, multipath parameterization may be the best choice since the temporal and spatial properties can be fully considered. Unfortunately, how to parameterize the multipath is still an urgent problem to be solved. Second, traditional multipath mitigation methods cannot work well in real-time or kinematic cases. If coupled with complex conditions, the multipath may become a dominant error source of unmodeled effects. The multipath always has apparent adverse effects when we conduct the MCAR, where the baseline length is usually long. Unfortunately, the multipath is always ignored in the MCAR.

We propose a new code and phase multipath parameterized mitigation method based on the observation domain. Specifically, the multi-frequency code multipath (MCM) and multi-frequency phase multipath (MPM) combinations are formed and preprocessed first in five or least four frequencies cases. After that, the multipath errors of code and phase observations are estimated by the least-squares (LS) criterion.

The main contribution of this research is twofold. First, the general models, methods of the MCAR, especially the FiCAR considering the multipath, are systematically studied. Second, a new code and phase multipath mitigation method is proposed and fully considered in the FiCAR.

According to the wavelength, the linear combinations can be defined as extra-wide lane (EWL, $\lambda \geq 2.93$ m), wide lane (WL, $0.75\ \text{m} \leq \lambda < 2.93$ m), medium lane (ML, $0.19\ \text{m} \leq \lambda < 0.75$ m), and narrow lane (NL, $0.10\ \text{m} \leq \lambda < 0.19$ m). The baseline length can be divided into three categories, including medium-to-short baseline ($l \leq 100$km), medium-to-long baseline ($100\ \text{km} < l \leq 200\ \text{km}$) and long baseline ($l > 200$ km). The symbols and operators used are described as follows. The symbols 'Δ' and '∇' denote the between-receiver and between-satellite SD operators, '$[.]_{\text{round}}$' denotes the rounding operator, 'diag' denotes the operator of a diagonal matrix, '$\mathbb{D}$' denotes the dispersion operator, and $\boldsymbol{I}$ denotes the identity matrix.

Five-frequency carrier ambiguity resolution

As an important part of the MCAR, the optimal linear combinations are studied comprehensively in this section. Then different FiCAR methods, including the GF FiCAR and GB FiCAR are discussed.

Five-frequency GNSS linear combination

If there are k ($k = 5$ in this study) frequencies satisfying $f_1 > f_2 > \cdots > f_k$ in multi-frequency GNSS, the frequency, wavelength, and DD ambiguities of a certain linear combination read

$$f_{[k]} = f_{(i_1,i_2,\cdots,i_k)} = i_1 \cdot f_1 + i_2 \cdot f_2 + \cdots + i_k \cdot f_k \tag{1}$$

$$\lambda_{[k]} = \lambda_{(i_1,i_2,\cdots,i_k)} = c/f_{[k]} \tag{2}$$

$$\nabla\Delta N_{[k]} = \nabla\Delta N_{(i_1,i_2,\cdots,i_k)} = i_1 \cdot \nabla\Delta N_1 + i_2 \cdot \nabla\Delta N_2 + \cdots + i_k \cdot \nabla\Delta N_k \tag{3}$$

where $i_1, i_2, \cdots, i_k$ are the integer coefficients, λ denotes the wavelength, c denotes the light speed in a vacuum, and N denotes the ambiguity. Accordingly, the linear code and phase combinations read

$$\nabla\Delta P_{[k]} = \nabla \cdot P_{(i_1,i_2,\cdots,i_k)} = \left(i_1 \cdot f_1 \cdot \nabla\Delta P_1 + i_2 \cdot f_2 \cdot \nabla\Delta P_2 + \cdots + i_k \cdot f_k \cdot \nabla\Delta P_k\right)/f_{[k]} \tag{4}$$

$$\nabla\Delta\Phi_{[k]} = \nabla\Delta\Phi_{(i_1,i_2,\cdots,i_k)} = \left(i_1 \cdot f_1 \cdot \nabla\Delta\Phi_1 + i_2 \cdot f_2 \cdot \nabla\Delta\Phi_2 + \cdots + i_k \cdot f_k \cdot \nabla\Delta\Phi_k\right)/f_{[k]} \tag{5}$$

where P and ϕ denote the code and phase observations, respectively. Then the observation models of linear code and phase combinations can be formed

$$\nabla\Delta P_{[k]} = \nabla\Delta\rho + \beta_{[k]}\nabla\Delta I_1 + \nabla\Delta T + \nabla\Delta M_{[k]} + \nabla\Delta\varepsilon_{[k]} \tag{6}$$

$$\nabla\Delta\Phi_{[k]} = \nabla\Delta\rho + \lambda_{[k]}\nabla\Delta N_{[k]} - \beta_{[k]}\nabla\Delta I_1 + \nabla\Delta T + \nabla\Delta m_{[k]} + \nabla\Delta e_{[k]} \tag{7}$$

with the first-order ionospheric scale factor $\beta_{[k]} = f_1^2\left(i_1/f_1 + i_2/f_2 + \cdots + i_k/f_k\right)/f_{[k]}$, where ρ denotes the receiver-to-satellite range, and I and T denote the ionospheric and tropospheric delays. M and m denote the code and phase multipath, and ε and e denote the code and phase observation noise.

Table 1 Information of the five-frequency BDS-3 signals

Signal type	Frequency (MHz)	Wavelength (cm)	Code chipping rate (Mcps)
B1C	1575.420	19.03	1.023
B1I	1561.098	19.20	2.046
B3I	1268.520	23.63	10.23
B2b	1207.140	24.83	10.23
B2a	1176.450	25.48	10.23

In the case of the five-frequency BDS-3 system, detailed information is listed in Table 1. It is worth noting that the code chipping rates of different signals are not the same. Hence the code precisions from different signals are also different. To obtain the optimal linear combination, the code and phase total noise levels (TNLs) are used. Since the baseline length is usually relatively long in MCAR, the second-order ionospheric delay and the orbit error should be better considered. Unlike the other traditional studies, here, the multipath is also considered in code and phase TNLs. The main reason is that the multipath may play an important role under complex conditions. Besides, the multipath is amplified in MCAR, which will be mentioned in the following test. The code TNL σ_{TN_P} and phase TNL σ_{TN_Φ} read

$$\sigma_{TN_P} = \sqrt{\beta_{[k]}^2\sigma_{\nabla\Delta I_1}^2 + \theta_{[k]}^2\sigma_{\nabla\Delta I_2}^2 + \sigma_{\nabla\Delta T}^2 + \mu_{[k]}^2\sigma_{\nabla\Delta M}^2 + \sigma_{\nabla\Delta O}^2 + \eta_{[k]}^2\sigma_{\varepsilon_{\nabla\Delta P}}^2} \tag{8}$$

$$\sigma_{TN_\Phi} = \sqrt{\beta_{[k]}^2\sigma_{\nabla\Delta I_1}^2 + \theta_{[k]}^2\sigma_{\nabla\Delta I_2}^2 + \sigma_{\nabla\Delta T}^2 + \mu_{[k]}^2\sigma_{\nabla\Delta m}^2 + \sigma_{\nabla\Delta O}^2 + \mu_{[k]}^2\sigma_{\varepsilon_{\nabla\Delta\Phi}}^2}/\lambda_{[k]} \tag{9}$$

with the second-order ionospheric scale factor $\theta_{[k]} = f_1^3\left(i_1/f_1^2 + i_2/f_2^2 + \cdots + i_k/f_k^2\right)/f_{[k]}$, the multipath and phase noise amplitude factor $\mu_{[k]}^2 = \left[\left(i_1 \bullet f_1\right)^2 + \left(i_2 \bullet f_2\right)^2 + \cdots + \left(i_k \bullet f_k\right)^2\right]/f_{[k]}^2$, the code noise amplitude factor $\eta_{[k]}^2 = \left[\left(i_1 \bullet f_1\right)^2 + \left(\alpha_{12} \bullet i_2 \bullet f_2\right)^2 + \cdots + \left(\alpha_{1k} \bullet i_k \bullet f_k\right)^2\right]/f_{[k]}^2$ where α_{1k} denotes the scale factor between the frequencies 1 and k. $\sigma_{\nabla\Delta I_1}$ and $\sigma_{\nabla\Delta I_2}$ denote the standard deviations (STDs) of the DD first-order and second-order ionospheric delays, $\nabla\Delta T$ denotes the STD of the DD tropospheric delay, $\nabla\Delta O$ denotes the STD of the DD orbit error, $\sigma_{\nabla\Delta M}$ and $\sigma_{\nabla\Delta m}$ denote the STDs of the DD code and phase multipath, and $\sigma_{\varepsilon_{\nabla\Delta P}}$ and $\sigma_{\varepsilon_{\nabla\Delta\Phi}}$ denote the STDs of the DD code and phase

Table 2 DD code and phase error budgets for the medium-to-short, medium-to-long, and long baselines (cm)

Error terms	Medium-to-short baseline	Medium-to-long baseline	Long baseline
Phase noise	1	1	1
Code noise on B1C	100	100	100
Phase multipath	1	1	1
Code multipath	100	100	100
1st-order ionospheric delay	10	40	100
2nd-order ionospheric delay	0.5	1	2
Tropospheric delay	1	2.5	20
Orbit error	0.5	1	10

noise. According to the code chipping rates listed in Table 1, without loss of generality, there has the relationship $\sigma_{\varepsilon_{\nabla\Delta P}} = \sigma_{\varepsilon_{\nabla\Delta P_1}} = \alpha_{12}\sigma_{\varepsilon_{\nabla\Delta P_2}} = \alpha_{13}\sigma_{\varepsilon_{\nabla\Delta P_3}} = \alpha_{14}\sigma_{\varepsilon_{\nabla\Delta P_4}} = \alpha_{15}\sigma_{\varepsilon_{\nabla\Delta P_5}}$ with empirical values $\alpha_{12} = 0.5$, $\alpha_{13} = 0.1$, $\alpha_{14} = 0.1$, and $\alpha_{15} = 0.1$; $\sigma_{\varepsilon_{\nabla\Delta\Phi}} = \sigma_{\varepsilon_{\nabla\Delta\Phi_1}} = \sigma_{\varepsilon_{\nabla\Delta\Phi_2}} = \sigma_{\varepsilon_{\nabla\Delta\Phi_3}} = \sigma_{\varepsilon_{\nabla\Delta\Phi_4}} = \sigma_{\varepsilon_{\nabla\Delta\Phi_5}}$. Similar processing approaches can be found in other research such as Tang et al. (2014) and Zhang et al. (2020).

In order to determine the optimal linear combinations, Table 2 presents the error budgets of different DD code and phase error types for different baseline lengths. The empirical values are widely adopted in other research (Li et al. 2010; Zhang et al. 2020). Unlike other related studies, the code and phase multipath effects are considered here. Then according to Tables 1 and 2, the wavelength of linear phase combinations can be computed by (1) and (2). Five independent combinations need to be determined in advance. Since only four independent combinations can be found under the conditions of $i_1 + i_2 + i_3 + i_4 + i_5 = 0$, the raw signal satisfying $i_1 + i_2 + i_3 + i_4 + i_5 = 1$ is treated as the fifth independent signal. It is worth noting that the correlations between the selected optimal liner combinations are often ignored in MCAR. The reason is that the EWL or WL is easy to be fixed directly due to their relatively low noise level and long wavelength. The four independent EWL/WL optimal linear phase combinations and NL optimal linear code combinations under different conditions can be found according to the TNLs. Tables 3 and 4 list the detailed information of the optimal linear phase and code combinations for the five-frequency BDS-3 system in this study.

FiCAR method

There are two main approaches in FiCAR. Specifically, one is the GF-FiCAR method, and the other one is the GB-FiCAR method. For the GF-FiCAR method, one can compute two main specific types

$$\nabla\Delta\check{N}_{\mathrm{LC1}} = \left[\left(\nabla\Delta P_{[k]} - \nabla\Delta\Phi_{\mathrm{LC1}}\right)/\lambda_{\mathrm{LC1}}\right]_{\mathrm{round}} \tag{10}$$

Table 3 Optimal linear phase combinations of five-frequency BDS-3 observations under the circumstances of medium-to-short, medium-to-long, and long baselines

Baseline length	i_1	i_2	i_3	i_4	i_5	$\lambda_{[5]}$(m)	σ_{TN_Φ}(cycle)
Medium to short	0	0	0	1	−1	9.7684	0.0815
	0	0	1	−1	0	4.8842	0.0892
	1	−1	0	0	0	20.9323	0.1047
	0	1	−1	0	0	1.0247	0.1558
Medium to long	1	−1	0	0	0	20.9323	0.1064
	0	0	0	1	−1	9.7684	0.1071
	0	0	1	−2	1	9.7684	0.1530
	0	1	−3	0	2	2.7646	0.2378
Long	1	−1	0	0	0	20.9323	0.1157
	−1	1	0	1	−1	18.3158	0.1859
	−1	1	1	−2	1	18.3158	0.2043
	0	1	−3	−1	3	3.8560	0.2693

Table 4 Optimal linear code combinations of five-frequency BDS-3 observations under the circumstances of medium-to-short, medium-to-long, and long baselines

Baseline length	i_1	i_2	i_3	i_4	i_5	σ_{TN_P}(m)
Medium to short	0	0	1	1	0	0.7293
Medium to long	0	1	1	0	0	0.9142
Long	0	1	1	0	0	1.4850

$$\nabla\Delta\check{N}_{\mathrm{LC2}} = \left[\left(\nabla\Delta\Phi_{\mathrm{LC1}} - \lambda_{\mathrm{LC1}}\cdot\nabla\Delta\underset{\mathrm{LC1}}{N} - \nabla\Delta\Phi_{\mathrm{LC2}}\right)/\lambda_{\mathrm{LC2}}\right]_{\mathrm{round}} \tag{11}$$

where the subscripts $LC1$ and $LC2$ denote the first and second linear phase combinations, and $\nabla\Delta N$ denotes the fixed DD integer ambiguities. The ambiguities of chosen linear combinations are fixed one by one according to the values of TNL or wavelength. In real applications, one can choose either (10) or (11) according to the precisions of $\nabla\Delta P_{[k]}$ and $\nabla\Delta\Phi_{LC1}$.

In the GB-FiCAR method, the three-dimensional coordinates are resolved together with the ambiguities. There have two main types

$$\begin{bmatrix} \boldsymbol{v}_{P_{[k]}} \\ \boldsymbol{v}_{LC1} \end{bmatrix} = \begin{bmatrix} \boldsymbol{A} & 0 \\ \boldsymbol{A} & \boldsymbol{I}\cdot\lambda_{LC1} \end{bmatrix} \begin{bmatrix} \boldsymbol{x} \\ \nabla\Delta\boldsymbol{N}_{LC1} \end{bmatrix} - \begin{bmatrix} \boldsymbol{l}_{P_{[k]}} \\ \boldsymbol{l}_{LC1} \end{bmatrix} \tag{12}$$

$$\begin{bmatrix} \boldsymbol{v}'_{LC1} \\ \boldsymbol{v}_{LC2} \end{bmatrix} = \begin{bmatrix} \boldsymbol{A} & 0 \\ \boldsymbol{A} & \boldsymbol{I}\cdot\lambda_{LC2} \end{bmatrix} \begin{bmatrix} \boldsymbol{x} \\ \nabla\Delta\boldsymbol{N}_{LC2} \end{bmatrix} - \begin{bmatrix} \boldsymbol{l}'_{LC1} \\ \boldsymbol{l}_{LC2} \end{bmatrix} \tag{13}$$

where the $\boldsymbol{v}$ and $\boldsymbol{v}'$ denote the residual and fixed residual vectors. $\boldsymbol{l}$ and $\boldsymbol{l}'$ denote the observation and fixed observation vectors, and $\boldsymbol{A}$ and $\boldsymbol{x}$ denote the design matrix and baseline component. Here, the ambiguities of chosen linear combinations are also fixed one by one through a certain sequence. Similarly, if the precision of $\boldsymbol{l}'_{LC1}$ is higher than that of $\boldsymbol{l}_P$, once can choose (13) to fix the ambiguities. It is also worth noting that more code or linear code combination observations can be used, thus making more redundant observations. Besides, the high-precision fixed NL can also be used in (13).

Multipath mitigation in multi-frequency code and phase observations

In this section, the amplification effects of code and phase multipath in five-frequency linear combinations are discussed. Then the theory and method of the new multipath parameterized mitigation method are proposed.

Multipath effects in five-frequency linear combinations

The code and phase multipath in multi-frequency linear combinations can be derived

$$\nabla\Delta M_{[k]} = \left(i_1\cdot f_1\cdot\nabla\Delta M_1 + i_2\cdot f_2\cdot\nabla\Delta M_2 + \cdots + i_k\cdot f_k\cdot\nabla\Delta M_k\right)/f_{[k]} \tag{14}$$

$$\nabla\Delta m_{[k]} = \left(i_1\cdot f_1\cdot\nabla\Delta m_1 + i_2\cdot f_2\cdot\nabla\Delta m_2 + \cdots + i_k\cdot f_k\cdot\nabla\Delta m_k\right)/f_{[k]} \tag{15}$$

Then the multipath factor can be obtained

$$\nu = \left(|i_1|\cdot f_1 + |i_2|\cdot f_2 + \cdots + |i_k|\cdot f_k\right)/f_{[k]} \tag{16}$$

The multipath factors and the wavelength magnifications for the wavelength of the optimal combination corresponding to the wavelength of each raw observation are presented in Table 5. It can be seen that the multipath factor is rather large, which can be up to 488.5. We can also find that the multipath factor of each optimal linear phase combination is larger than the wavelength magnifications. Specifically, the multipath factors are approximately 2.0, 3.4, and 5.0 times of wavelength magnifications under the circumstances of medium-to-short, medium-to-long, and long baselines, respectively. This value can be up to 8.6 times, where the multipath cannot be ignored apparently. It indicates that the multipath will be more significant in optimal linear phase combinations, especially in long baselines. Unfortunately, the FiCAR at this time usually cannot work best. Therefore, it is highly urgent to mitigate the multipath in FiCAR.

A new parameterization method for mitigation code and phase multipath

To mitigate the code and phase multipath by observation-domain parameterization, starting from the UD and uncombined observation equations, the between-receiver SD MCM

Table 5 Multipath factors and the wavelength magnifications for the wavelength of the optimal combination corresponding to the wavelength of each raw observation under the circumstances of medium-to-short, medium-to-long, and long baselines

Baseline length	Linear combination	ν	B1C	B1I	B3I	B2b	B2a
Medium to short	$\nabla\Delta\Phi_{(0,0,0,1,-1)}$	77.67	51.33	50.87	41.33	39.33	38.33
	$\nabla\Delta\Phi_{(0,0,1,-1,0)}$	40.33	25.67	25.43	20.67	19.67	19.17
	$\nabla\Delta\Phi_{(1,-1,0,0,0)}$	219.00	110.00	109.00	88.57	84.29	82.14
	$\nabla\Delta\Phi_{(0,1,-1,0,0)}$	9.67	5.38	5.34	4.34	4.13	4.02
Medium to long	$\nabla\Delta\Phi_{(1,-1,0,0,0)}$	219.00	110.00	109.00	88.57	84.29	82.14
	$\nabla\Delta\Phi_{(0,0,0,1,-1)}$	77.67	51.33	50.87	41.33	39.33	38.33
	$\nabla\Delta\Phi_{(0,0,1,-2,1)}$	158.33	51.33	50.87	41.33	39.33	38.33
	$\nabla\Delta\Phi_{(0,1,-3,0,2)}$	71.19	14.53	14.40	11.70	11.13	10.85
Long	$\nabla\Delta\Phi_{(1,-1,0,0,0)}$	219.00	110.00	109.00	88.57	84.29	82.14
	$\nabla\Delta\Phi_{(-1,1,0,1,-1)}$	337.25	96.25	95.38	77.50	73.75	71.87
	$\nabla\Delta\Phi_{(-1,1,1,-2,1)}$	488.50	96.25	95.38	77.50	73.75	71.87
	$\nabla\Delta\Phi_{(0,1,-3,-1,3)}$	129.95	20.26	20.08	16.32	15.53	15.13

and SD MPM combinations are formulated, which eliminate the clock offset and hardware delay of the satellite. In addition, since the SD MCM and SD MPM combinations are the GF and IF combinations, there only leave the receiver-dependent code and phase hardware delays, the code and phase multipath, and the observation noise. The ambiguities are also existent in SD MPM combinations. The between-receiver SD MCM and SD MPM combinations read

$$\begin{aligned}\Delta\mathrm{MCM}_{\mathrm{ijk}} &= \left(\lambda_k^2-\lambda_j^2\right)\Delta P_i+\left(\lambda_i^2-\lambda_k^2\right)\Delta P_j+\left(\lambda_j^2-\lambda_i^2\right)\Delta P_k=\left(\lambda_k^2-\lambda_j^2\right)\Delta\xi_i+\left(\lambda_i^2-\lambda_k^2\right)\Delta\xi_j\\&+\left(\lambda_j^2-\lambda_i^2\right)\Delta\xi_k+\left(\lambda_k^2-\lambda_j^2\right)\Delta M_i+\left(\lambda_i^2-\lambda_k^2\right)\Delta M_j+\left(\lambda_j^2-\lambda_i^2\right)\Delta M_k+\varepsilon_{\Delta\mathrm{MCM}_{\mathrm{ijk}}}\end{aligned} \tag{17}$$

$$\begin{aligned}\Delta\mathrm{MPM}_{\mathrm{ijk}} &= \left(\lambda_k^2-\lambda_j^2\right)\Delta\phi_i+\left(\lambda_i^2-\lambda_k^2\right)\Delta\phi_j+\left(\lambda_j^2-\lambda_i^2\right)\Delta\phi_k=\left(\lambda_k^2-\lambda_j^2\right)\lambda_i\Delta N_i+\left(\lambda_i^2-\lambda_k^2\right)\lambda_j\Delta N_j\\&+\left(\lambda_j^2-\lambda_i^2\right)\lambda_k\Delta N_k+\left(\lambda_k^2-\lambda_j^2\right)\Delta\zeta_i+\left(\lambda_i^2-\lambda_k^2\right)\Delta\zeta_j+\left(\lambda_j^2-\lambda_i^2\right)\Delta\zeta_k+\left(\lambda_k^2-\lambda_j^2\right)\Delta m_i\\&+\left(\lambda_i^2-\lambda_k^2\right)\Delta m_j+\left(\lambda_j^2-\lambda_i^2\right)\Delta m_k+e_{\Delta\mathrm{MPM}_{\mathrm{ijk}}}\end{aligned} \tag{18}$$

where the subscripts i, j and k denote the frequencies,ξ and ζ denote the code and phase hardware delays. $\varepsilon_{\Delta\mathrm{MCM}_{ijk}}$ and $e_{\Delta\mathrm{MPM}_{ijk}}$ denote the noise of $\Delta\mathrm{MCM}_{ijk}$ and $\Delta\mathrm{MPM}_{ijk}$. The SD code and phase hardware delays and the SD ambiguities need to be removed to estimate the SD code and phase multipath in (17) and (18). Since the hardware delays and the ambiguities can be regarded as a constant if there are no cycle slips within a certain period (de Bakker et al. 2012; Cai et al. 2016), the method of removing the averages over a certain period is used. Therefore, the preprocessed SD MCM ($\Delta\mathrm{MCM}'_{ijk}$) and SD MPM ($\Delta\mathrm{MPM}'_{ijk}$) combinations can be computed

$$\begin{aligned}\Delta\mathrm{MCM}'_{\mathrm{ijk}} &= \left(\lambda_k^2-\lambda_j^2\right)\Delta P_i+\left(\lambda_i^2-\lambda_k^2\right)\Delta P_j+\left(\lambda_j^2-\lambda_i^2\right)\Delta P_k-\frac{1}{n}\sum_{t=1}^{n}\left[\Delta\mathrm{MCM}_{\mathrm{ijk}}(t)\right]\\&=\left(\lambda_k^2-\lambda_j^2\right)\Delta M_i+\left(\lambda_i^2-\lambda_k^2\right)\Delta M_j+\left(\lambda_j^2-\lambda_i^2\right)\Delta M_k+\varepsilon_{\Delta\mathrm{MCM}_{\mathrm{ijk}}}\end{aligned} \tag{19}$$

$$\begin{aligned}\Delta\mathrm{MPM}'_{\mathrm{ijk}} &= \left(\lambda_k^2-\lambda_j^2\right)\Delta\phi_i+\left(\lambda_i^2-\lambda_k^2\right)\Delta\phi_j+\left(\lambda_j^2-\lambda_i^2\right)\Delta\phi_k-\frac{1}{n}\sum_{t=1}^{n}\left[\Delta\mathrm{MPM}_{\mathrm{ijk}}(t)\right]\\&=\left(\lambda_k^2-\lambda_j^2\right)\Delta m_i+\left(\lambda_i^2-\lambda_k^2\right)\Delta m_j+\left(\lambda_j^2-\lambda_i^2\right)\Delta m_k+e_{\Delta\mathrm{MPM}_{\mathrm{ijk}}}\end{aligned} \tag{20}$$

In the case of five frequencies, 10 different SD MCM and SD MPM combinations can be formed with different frequency combinations in a single epoch. Since there are only 5 SD code and phase multipaths to be determined for a certain satellite, these SD code and phase multipath can be parameterized and estimated by the LS criterion. It is worth noting that 4 different SD MCM and SD MPM combinations can be formed when there are four frequencies. Accordingly, four unknown SD code and phase multipath can be uniquely determined. That is, the proposed procedure can be used in at least four-frequency situation. It is worth noting that the UD or DD MCM and MPM multipath combinations can also be formed and estimated in a similar way. The reason why the SD MCM and MPM combinations are used here is that they are more suitable for the relative mode and are not affected by the reference satellite.

Taking the five-frequency case as an example, the specific steps of multipath parameterization are as follows. First, the code and phase functional models of UD, SD or DD multipath parameterization can be derived

$$\mathbf{MCM}=\mathbf{BM}+\boldsymbol{\varepsilon} \tag{21}$$

$$\mathbf{MPM}=\mathbf{Bm}+\boldsymbol{e} \tag{22}$$

where **MCM** and **MPM** denote the preprocessed MCM and MPM observation vectors, respectively. $\boldsymbol{B}$ denotes the design matrix, $\boldsymbol{M}$ and $\boldsymbol{m}$ denote the code and phase multipath vectors to be estimated. $\boldsymbol{\varepsilon}$ and $\boldsymbol{e}$ denote the noise vectors of **MCM** and **MPM**. Then the (21) and (22) can be expanded to

$$\begin{bmatrix} \mathrm{MCM}'_{123} \\ \mathrm{MCM}'_{124} \\ \mathrm{MCM}'_{125} \\ \mathrm{MCM}'_{134} \\ \mathrm{MCM}'_{135} \\ \mathrm{MCM}'_{145} \\ \mathrm{MCM}'_{234} \\ \mathrm{MCM}'_{235} \\ \mathrm{MCM}'_{245} \\ \mathrm{MCM}'_{345} \end{bmatrix} = \begin{bmatrix} \alpha_{32} & \alpha_{13} & \alpha_{21} & 0 & 0 \\ \alpha_{42} & \alpha_{14} & 0 & \alpha_{21} & 0 \\ \alpha_{52} & \alpha_{15} & 0 & 0 & \alpha_{21} \\ \alpha_{43} & 0 & \alpha_{14} & \alpha_{31} & 0 \\ \alpha_{53} & 0 & \alpha_{15} & 0 & \alpha_{31} \\ \alpha_{54} & 0 & 0 & \alpha_{15} & \alpha_{41} \\ 0 & \alpha_{43} & \alpha_{24} & \alpha_{32} & 0 \\ 0 & \alpha_{53} & \alpha_{25} & 0 & \alpha_{32} \\ 0 & \alpha_{54} & 0 & \alpha_{25} & \alpha_{42} \\ 0 & 0 & \alpha_{54} & \alpha_{35} & \alpha_{43} \end{bmatrix} \begin{bmatrix} M_1 \\ M_2 \\ M_3 \\ M_4 \\ M_5 \end{bmatrix} + \begin{bmatrix} \varepsilon_{\mathrm{MCM}_{123}} \\ \varepsilon_{\mathrm{MCM}_{124}} \\ \varepsilon_{\mathrm{MCM}_{125}} \\ \varepsilon_{\mathrm{MCM}_{134}} \\ \varepsilon_{\mathrm{MCM}_{135}} \\ \varepsilon_{\mathrm{MCM}_{145}} \\ \varepsilon_{\mathrm{MCM}_{234}} \\ \varepsilon_{\mathrm{MCM}_{235}} \\ \varepsilon_{\mathrm{MCM}_{245}} \\ \varepsilon_{\mathrm{MCM}_{345}} \end{bmatrix} \tag{23}$$

$$\begin{bmatrix} \mathrm{MPM}'_{123} \\ \mathrm{MPM}'_{124} \\ \mathrm{MPM}'_{125} \\ \mathrm{MPM}'_{134} \\ \mathrm{MPM}'_{135} \\ \mathrm{MPM}'_{145} \\ \mathrm{MPM}'_{234} \\ \mathrm{MPM}'_{235} \\ \mathrm{MPM}'_{245} \\ \mathrm{MPM}'_{345} \end{bmatrix} = \begin{bmatrix} \alpha_{32} & \alpha_{13} & \alpha_{21} & 0 & 0 \\ \alpha_{42} & \alpha_{14} & 0 & \alpha_{21} & 0 \\ \alpha_{52} & \alpha_{15} & 0 & 0 & \alpha_{21} \\ \alpha_{43} & 0 & \alpha_{14} & \alpha_{31} & 0 \\ \alpha_{53} & 0 & \alpha_{15} & 0 & \alpha_{31} \\ \alpha_{54} & 0 & 0 & \alpha_{15} & \alpha_{41} \\ 0 & \alpha_{43} & \alpha_{24} & \alpha_{32} & 0 \\ 0 & \alpha_{53} & \alpha_{25} & 0 & \alpha_{32} \\ 0 & \alpha_{54} & 0 & \alpha_{25} & \alpha_{42} \\ 0 & 0 & \alpha_{54} & \alpha_{35} & \alpha_{43} \end{bmatrix} \begin{bmatrix} m_1 \\ m_2 \\ m_3 \\ m_4 \\ m_5 \end{bmatrix} + \begin{bmatrix} e_{\mathrm{MPM}_{123}} \\ e_{\mathrm{MPM}_{124}} \\ e_{\mathrm{MPM}_{125}} \\ e_{\mathrm{MPM}_{134}} \\ e_{\mathrm{MPM}_{135}} \\ e_{\mathrm{MPM}_{145}} \\ e_{\mathrm{MPM}_{234}} \\ e_{\mathrm{MPM}_{235}} \\ e_{\mathrm{MPM}_{245}} \\ e_{\mathrm{MPM}_{345}} \end{bmatrix} \tag{24}$$

with $\alpha_{ij} = \lambda_i^2 - \lambda_j^2$ ($\alpha_{21} = 0$ in this study). According to the law of covariance propagation, the corresponding stochastic models read

$$\mathbb{D}(\mathbf{MCM}) = \sigma_{\Delta P}^2 \mathrm{diag}\left(\gamma_{123}, \gamma_{124}, \cdots, \gamma_{345}\right) \tag{25}$$

$$\mathbb{D}(\mathbf{MPM}) = \sigma_{\Delta\Phi}^2 \mathrm{diag}\left(\gamma_{123}, \gamma_{124}, \cdots, \gamma_{345}\right) \tag{26}$$

with $\gamma_{ijk} = \left(\lambda_k^2 - \lambda_j^2\right)^2 + \left(\lambda_i^2 - \lambda_k^2\right)^2 + \left(\lambda_j^2 - \lambda_i^2\right)^2$. It is worth noting that a fully populated stochastic model can also be used here if necessary. At last, the code and phase multipath can be estimated based on the LS criterion

$$\boldsymbol{M} = \left[\boldsymbol{B}^{\mathrm{T}}[\mathbb{D}(\mathbf{MCM})]^{-1}\boldsymbol{B}\right]^{-1}\boldsymbol{B}^{\mathrm{T}}[\mathbb{D}(\mathbf{MCM})]^{-1}\mathbf{MCM} \tag{27}$$

$$\boldsymbol{m} = \left[\boldsymbol{B}^{\mathrm{T}}[\mathbb{D}(\mathbf{MPM})]^{-1}\boldsymbol{B}\right]^{-1}\boldsymbol{B}^{\mathrm{T}}[\mathbb{D}(\mathbf{MPM})]^{-1}\mathbf{MPM} \tag{28}$$

After the multipath corrections are estimated, the multipath-reduced observations can be obtained. Theoretically, the multipath effects will be mitigated to a great extent in the FiCAR when using the multipath-reduced DD observations. Compared with other traditional methods, the parameterization method can be conducted based on the UD, SD, and DD modes in real-time or kinematic situations.

Test on real observations and result analysis

To evaluate and verify the performance of the proposed method, two baselines with different lengths were tested. The Trimble receivers were used as the reference and rover stations, where the 1-Hz five-frequency BDS-3 code and phase observations were collected. The high-end antennas with chokes are adopted in the reference stations and placed on the roof, whereas the low-cost antenna without a choke is placed in relatively obstructed places. Hence, the multipath effects are existent. Table 6 lists the detailed information of the baselines. It indicates that the two different baselines can represent two typical baseline lengths in single-baseline RTK or network RTK.

The traditional and improved FiCAR methods are both applied and compared. Four different AR modes are used in each type of FiCAR method, i.e., single-epoch GF FiCAR, single-epoch GB FiCAR, multi-epoch GF FiCAR, and multi-epoch GB FiCAR. The fixing strategy is rounding. The modified Hopfield model and ionospheric-fixed model are used. The cycle slips have been detected and repaired (Zhang and Li 2020). The true ambiguities are validated by comparing the fixed baseline solutions with the precise coordinates in advance. According to the total noise level, the first to fourth signals to be fixed are $\nabla\Delta\Phi_{(0,0,0,1,-1)}$, $\nabla\Delta\Phi_{(0,0,1,-1,0)}$, $\nabla\Delta\Phi_{(1,-1,0,0,0)}$ and $\nabla\Delta\Phi_{(0,1,-1,0,0)}$, then the fifth independent signal is $\nabla\Delta\Phi_{(0,0,0,0,1)}$. The optimal linear code combination $\nabla\Delta P_{(0,0,1,1,0)}$ is used as the precise code observation. The fixed $\nabla\Delta\Phi_{(0,0,1,-1,0)}$ is used as another precise signal. To further improve the success rate, in the single-epoch mode, the AR of the fifth signal may rely on the high-precision fixed NL $\nabla\Delta\Phi_{(4,4,-3,-3,-2)}$ of which the wavelength and precision are as small as 0.1084 and 0.1420 m, respectively. Here the ambiguities of $\nabla\Delta\Phi_{(4,4,-3,-3,-2)}$ can be computed directly with the above four EWLs. In the multi-epoch mode, the AR is set to reinitialize every 5 min. To avoid the potential sudden changes of the float solutions caused by the NL $\nabla\Delta\Phi_{(4,4,-3,-3,-2)}$, the AR of the fifth signal in multi-epoch mode is only assisted by the fixed $\nabla\Delta\Phi_{(0,0,1,-1,0)}$.

As an example, $\Delta\mathrm{MCM}_{123}$ and $\Delta\mathrm{MPM}_{123}$ as well as the elevation for PRN 36 are illustrated in Figs. 1 and 2, respectively. It can be found that the SD MCM and SD MPM combinations are rather stable during this period. Hence, it is feasible to avoid the impacts of the hardware delays and the ambiguities by removing the average in a certain period, e.g., 3 h in this study. The SD MCM or the SD MPM

Table 6 Details of the baselines used in the test

Baseline	Length	Duration
No.1	27.58 km	3 h
No.2	61.59 km	3 h

combinations from different baselines are highly consistent. It demonstrates that the distance-independent SD code and phase multipath effects are apparently existent and even dominant here.

Figures 3, 4, 5 and 6 show the $\Delta MCM'_{123}$, $\Delta MCM'_{145}$, $\Delta MPM'_{123}$ and $\Delta MPM'_{145}$, hence the information of all five frequencies is included. Each color denotes one satellite in each panel. It can be clearly seen that all the preprocessed SD MCM combinations fluctuate between −0.16 and 0.16 m regardless of the satellite and baseline length. Similar conclusions can be found in the preprocessed SD MPM combinations, of which the values fluctuate between −0.16 and 0.16 cm.

Figures 7 and 8 illustrate the SD code and phase multipath of the two baselines. We can find that all the code and phase multipath effects from different frequencies and baselines fluctuate between −4 and 4 m and −4 and 4 cm, respectively. Once again, since there are no significant differences between the two baselines, the site-specific multipath effects are indeed estimated.

Figure 9 illustrates the float solutions of the first four EWLs for baseline No.2 using traditional and improved

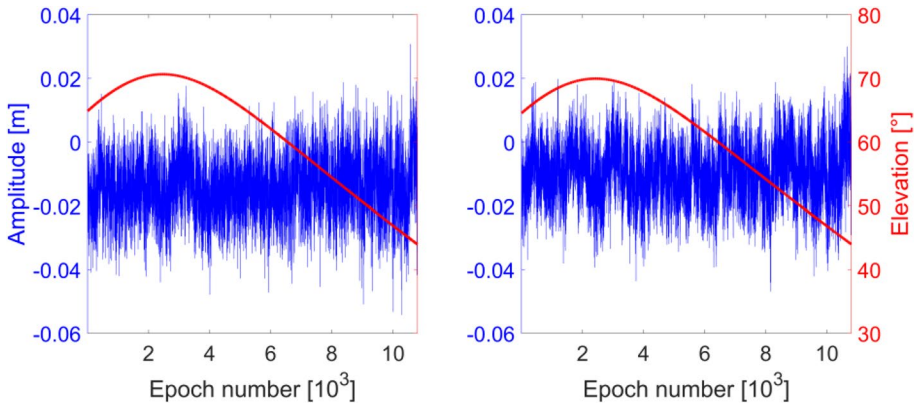

Fig. 1 SD MCM combination (blue) and elevation (red) of B1C, B1I, and B3I for PRN 36, where the left and right panels denote the results of baselines No.1 and 2, respectively

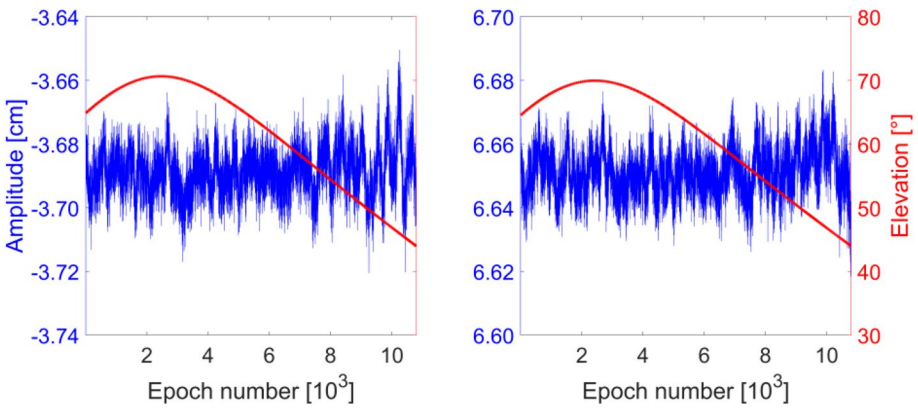

Fig. 2 SD MPM combination (blue) and elevation (red) of B1C, B1I, and B3I for PRN 36, where the left and right panels denote the results of baselines No.1 and 2, respectively

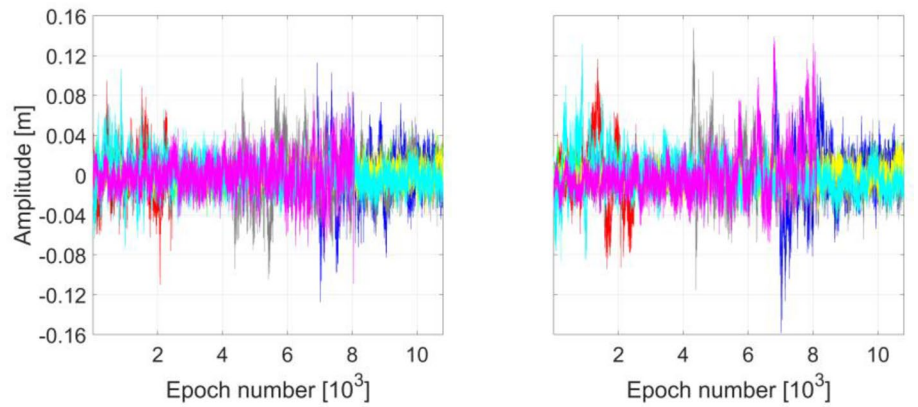

Fig. 3 Preprocessed SD MCM combination of B1C, B1I, and B3I, where the left and right panels denote the results of baselines No.1 and 2, respectively. Each color denotes one satellite

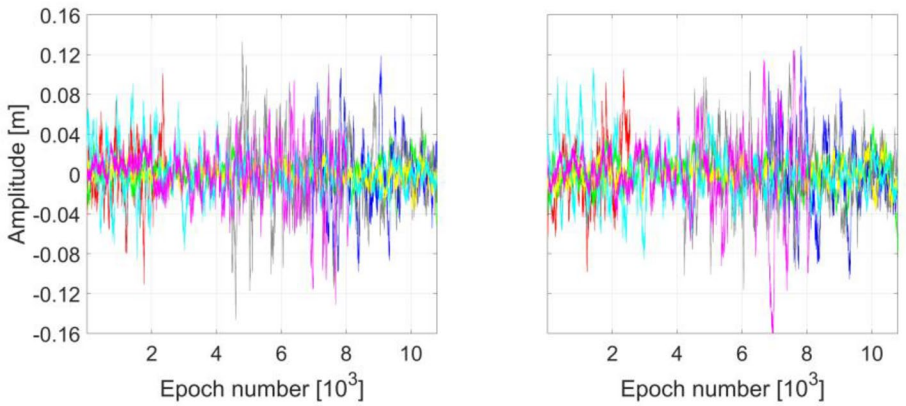

Fig. 4 Preprocessed SD MCM combination of B1C, B2b, and B2a, where the left and right panels denote the results of baselines No.1 and 2, respectively. Each color denotes one satellite

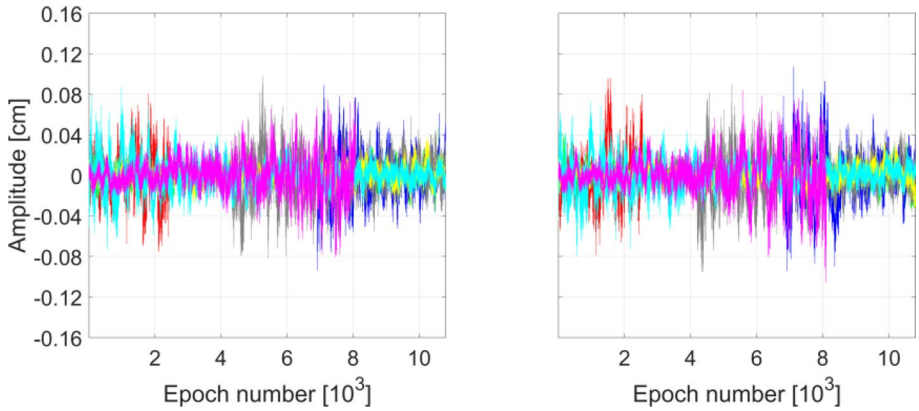

Fig. 5 Preprocessed SD MPM combination of B1C, B1I, and B3I, where the left and right panels denote the results of baselines No.1 and 2, respectively. Each color denotes one satellite

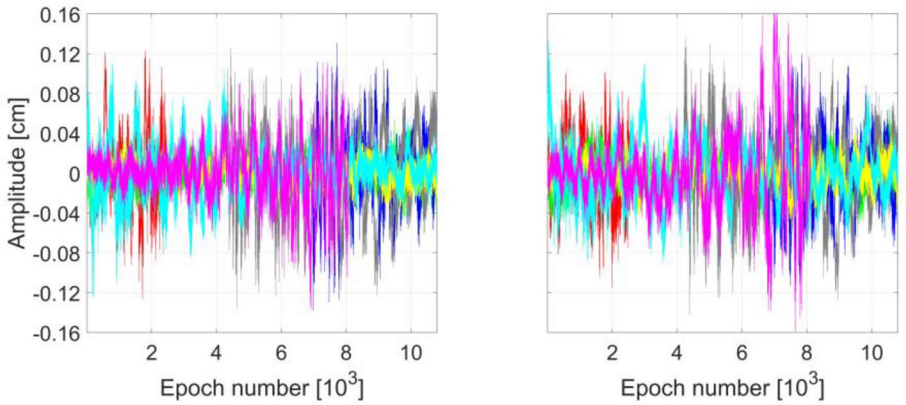

Fig. 6 Preprocessed SD MPM combination of B1C, B2b, and B2a, where the left and right panels denote the results of baselines No.1 and 2, respectively. Each color denotes one satellite

methods in the single-epoch GF-FiCAR mode. The panels in the same row denote one satellite pair. Similar conclusions can be found in baseline No.1 or GB-FiCAR mode. First, it can be clearly seen that all the ambiguities of the first three EWLs can be easily fixed by using either the traditional or improved methods. This is because the first three optimal phase liner combinations have enough small TNLs (i.e., only 0.0815, 0.0892, and 0.1047 cycles, respectively), and can weaken the influences of the multipath effects to a great extent. The proposed method has a better performance. For the fourth EWL, the proposed method can still fix the ambiguities easily, whereas the traditional method cannot. It can also be found that after the fixed EWL $\nabla\Delta\Phi_{(0,0,1,-1,0)}$ is used as the precise observation in the third and fourth signals, the float solutions of the proposed method have much better behaviors than those of the traditional method. It is reasonable that the multipath effects are mitigated to a great extent in the ionospheric-reduced signals. The results also indicate that since the proposed method can work much better than the traditional method, the proposed method can be used under complex conditions.

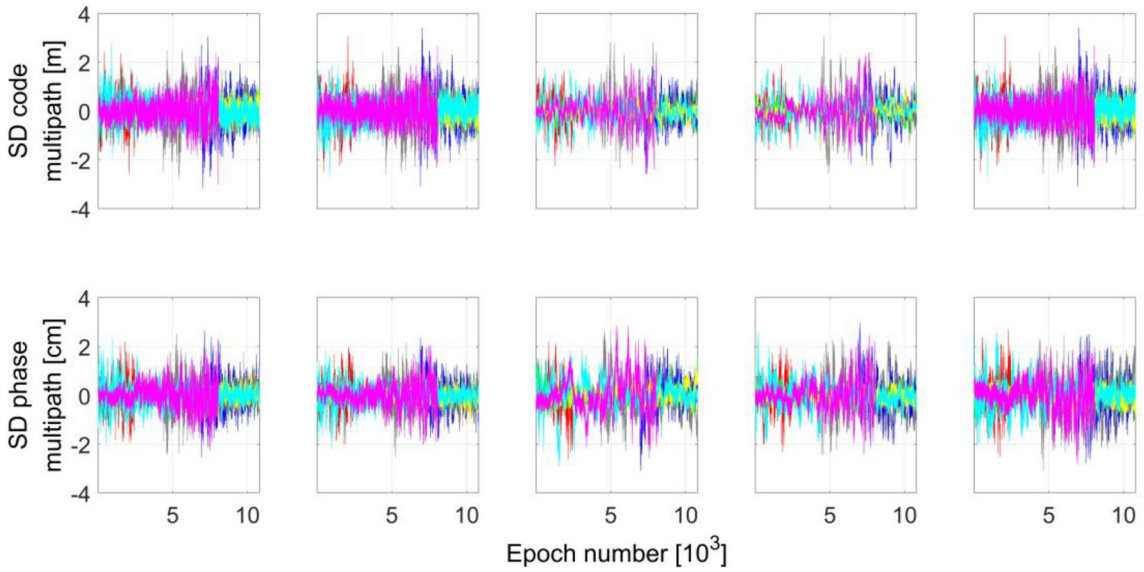

Fig. 7 SD code (up) and phase (bottom) multipath of each frequency for baseline No.1, where the left to right panels denote the results of B1C, B1I, B3I, B2b, and B2a, respectively. Each color denotes one satellite

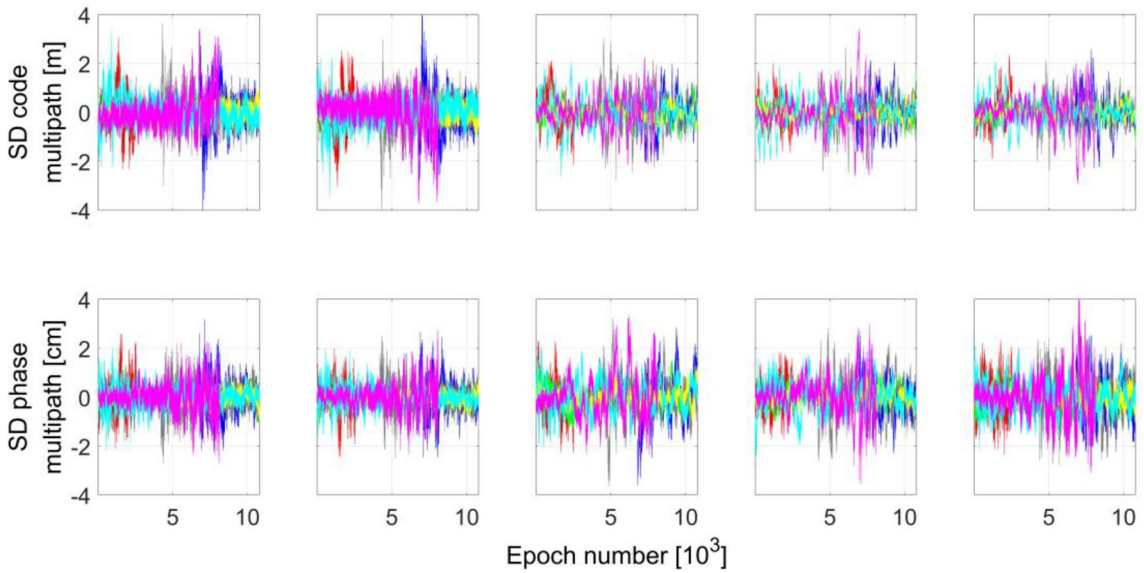

Fig. 8 SD code (up) and phase (bottom) multipath of each frequency for baseline No.2, where the left to right panels denote the results of B1C, B1I, B3I, B2b, and B2a, respectively. Each color denotes one satellite

Figure 10 shows the results of the fifth signal for baseline No.2 where the methods without NL assistance and with NL assistance are both tested. Once again, the float solutions of the proposed method are much better than the ones of the traditional method. Specifically, when there is no NL assistance, the fluctuations of the proposed method are much smaller than those of the traditional method. If the NL is used in FiCAR, the impacts of the multipath effects can be reduced. The main reason is that, as aforementioned, the multipath effects are significantly increased in EWL/WL. However, the shortcoming of the NL assistance is that it highly relies on the accuracy of the previously fixed ambiguities. Otherwise, there may exist sudden changes in the float solutions. Therefore, only the proposed method can simultaneously obtain a better AR performance without the potential problem of ambiguity jump.

Tables 7 and 8 present the root mean square (RMS) values between the float and true ambiguities for all the satellite

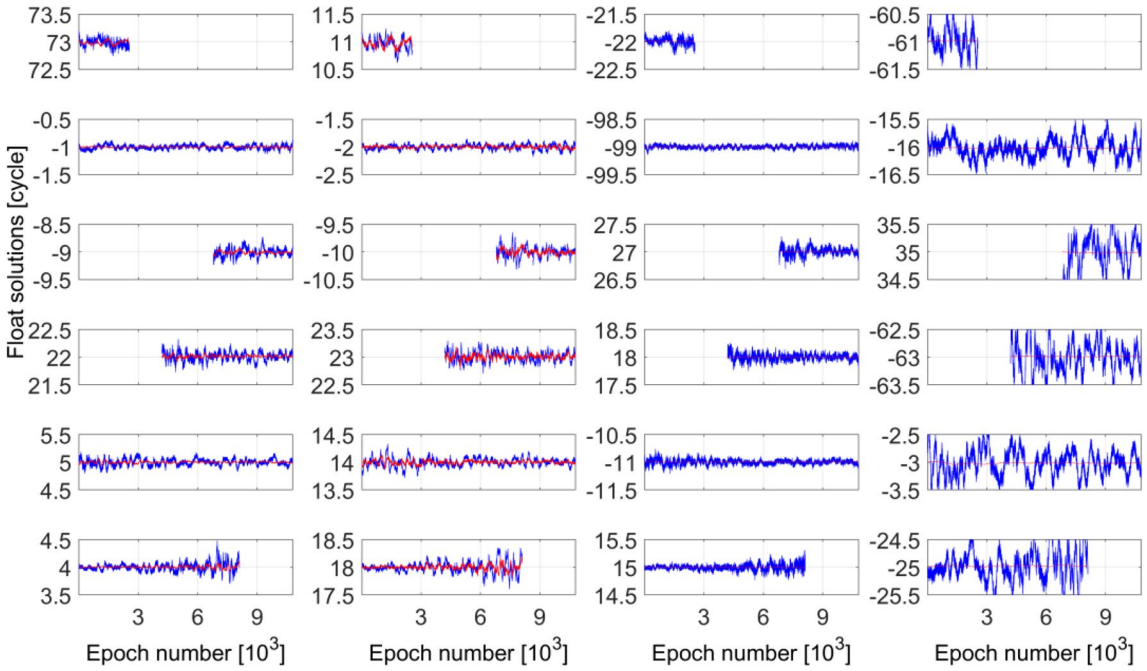

Fig. 9 Float solutions of the traditional (blue) and improved (red) methods for baseline No.2, where the left to right panels denote the results of $\nabla\Delta\Phi_{(0,0,0,1,-1)}$, $\nabla\Delta\Phi_{(0,0,1,-1,0)}$, $\nabla\Delta\Phi_{(1,-1,0,0,0)}$, and $\nabla\Delta\Phi_{(0,1,-1,0,0)}$. Four panels in the same row denote one satellite pair

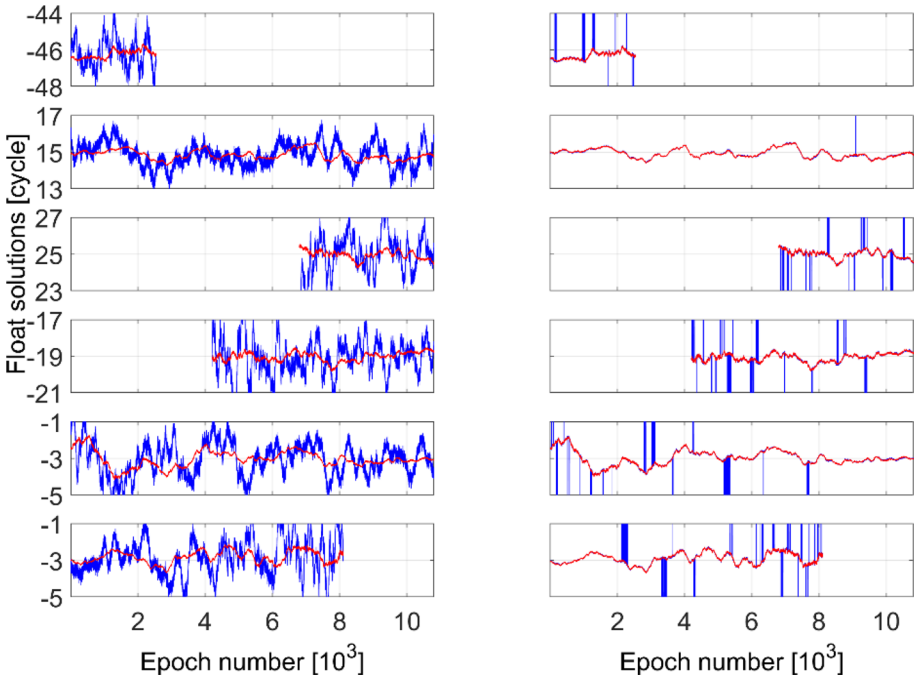

Fig. 10 Float solutions of the traditional (blue) and improved (red) methods for baseline No.2, where the left to right panels denote the results of the methods without NL assistance and with NL assistance. Two panels in the same row denote one satellite pair

pairs. The numbers 1–5 denote the first to fifth signals to be fixed. It can be found that the RMS values of the first three signals are all smaller than 0.07 cycles. Hence, it indicates that the ambiguities can be fixed with high reliability by both the traditional and improved methods. Compared with the RMS of the traditional method, where the mean value is approximately 0.0439 cycles, and the one of the proposed methods is only 0.0158 cycles. The improvement is as much as 64.0%. For the fourth signal, the RMS values can also be reduced significantly, where the mean values of the traditional and improved methods are 0.1602 and 0.0292 cycles, respectively. The results are consistent with the analysis

Table 7 RMS between the float and true ambiguities for all the satellite pairs by the traditional and improved methods, including the single-epoch GF-FiCAR and GB-FiCAR modes for baseline No.1 (cycle)

Method	1	2	3	4	5 without NL	5 with NL
Traditional GF	0.0468	0.0636	0.0389	0.1723	0.6403	0.5248
Improved GF	0.0145	0.0270	0.0018	0.0295	0.2670	0.1950
Traditional GB	0.0340	0.0373	0.0347	0.1326	0.2637	0.4613
Improved GB	0.0126	0.0243	0.0058	0.0374	0.2456	0.1702

Table 8 RMS between the float and true ambiguities for all the satellite pairs by the traditional and improved methods, including the single-epoch GF-FiCAR and GB-FiCAR modes for baseline No.2 (cycle)

Method	1	2	3	4	5 without NL	5 with NL
Traditional GF	0.0515	0.0660	0.0415	0.1949	0.7210	0.5860
Improved GF	0.0169	0.0326	0.0022	0.0161	0.2627	0.2375
Traditional GB	0.0361	0.0410	0.0355	0.1411	0.2641	0.4836
Improved GB	0.0151	0.0298	0.0074	0.0336	0.2395	0.1998

Table 9 Single-epoch AR success rates by the traditional and improved methods including the GF and GB modes for baseline No.1

Method	1	2	3	4	5 without NL	5 with NL
Traditional GF	100%	100%	100%	86.62%	9.81%	71.32%
Improved GF	100%	100%	100%	100%	51.38%	82.18%
Traditional GB	100%	100%	100%	93.96%	54.20%	73.70%
Improved GB	100%	100%	100%	100%	57.24%	87.19%

Table 10 Single-epoch AR success rates by the traditional and improved methods including the GF and GB modes for baseline No.2

Method	1	2	3	4	5 without NL	5 with NL
Traditional GF	100%	100%	100%	82.67%	4.80%	54.69%
Improved GF	100%	100%	100%	100%	55.49%	67.19%
Traditional GB	100%	100%	100%	93.54%	53.21%	58.15%
Improved GB	100%	100%	100%	100%	57.32%	77.12%

mentioned above. When fixing the fifth signal, it can be found that the traditional method cannot fix the ambiguities well. The traditional GF-FiCAR method is the worst among all these methods, and the improved GB-FiCAR method is the best. In addition, the method with NL assistance is generally better than the method without NL assistance, except for the traditional GB-FiCAR method. It is because that the traditional GB-FiCAR method can resist the impacts of unmodeled errors, including the multipath, to a great extent.

In the single-epoch process strategy, the indicator AR success rate $P = \left(n_{suc}/n_{tot}\right) \times 100\%$ is used with n_{suc} and n_{tot} denoting the epoch numbers of successful AR and the total epochs, respectively. The AR success rates by the traditional and improved methods are shown in Tables 9 and 10. From these tables, all the AR success rates of the first to third signals are 100%. For the fourth signal, the AR success rates of the proposed method can still reach 100%, whereas the traditional method cannot. The mean AR success rates of the traditional GF-FiCAR and GB-FiCAR methods are approximately 84.65% and 93.75%, respectively. Then for the fifth signal, the improved method can still slightly increase AR success rates, especially in the GF mode without NL assistance, where the maximum improvement can reach 50.7%. It again proves the effectiveness of the proposed method, which is especially useful for the last two signals.

If the ambiguities cannot be fixed instantaneously, the multi-epoch processing strategy may be used. The traditional and improved methods, including GF and GB modes for baselines No.1 and 2 are all tested. The time to first fix (TTFF) is used, where the critical thresholds of fraction and STD are set to ±0.2 and 0.1 cycles, respectively (Zhang et al. 2020). Table 11 presents the mean TTFF of all the satellite pairs calculated from each liner combination. We can find that the TTFF of the first to fourth signals by using the

Table 11 TTFF by the traditional and improved methods including GF and GB modes for baselines No.1 and 2 (s)

Method	No.1					No.2				
	1	2	3	4	5	1	2	3	4	5
Traditional GF	1.15	21.43	1.01	70.23	208.00	1.02	4.91	1.00	74.66	245.21
Improved GF	1.00	1.00	1.00	1.00	177.17	1.00	1.00	1.00	1.00	136.92
Traditional GB	1.00	1.13	1.00	56.67	153.34	1.16	1.00	1.00	53.60	165.41
Improved GB	1.00	1.00	1.00	1.00	133.26	1.00	1.00	1.00	1.00	129.97

improved method is 1.00 s, whereas the corresponding TTFF by using the traditional method ranges from 1.00 to 74.66 s. For the fifth signal, the mean TTFF values of the traditional and improved methods are approximately 193.0 and 144.3 s, respectively. In conclusion, the new multipath mitigation method is indeed effective.

Concluding remarks

We first propose a code and phase multipath mitigation method based on the observation-domain parameterization, which can be used in the FCAR and FiCAR. First, the basic theory and method of the MCAR, especially the FiCAR, are given. Second, the multipath effects in FiCAR are discussed. We can find that the presence of multipath may lead to difficulty in MCAR. Finally, the methodology of the multipath mitigation method is proposed. Specifically, different MCM and MPM from different frequencies are formed and preprocessed appropriately. Then the code and phase multipath are estimated based on the LS criterion.

To validate the effectiveness of the proposed method, the real five-frequency BDS-3 observations are applied. The single-epoch GF-FiCAR and GB-FiCAR, and multi-epoch GF-FiCAR and GB-FiCAR modes are all tested. According to the results, it can be concluded that the proposed method can indeed improve AR performance. First, the RMS values of the signals to be fixed by the proposed method are all smaller than the traditional method. Second, for the first four signals, only the AR success rates of the proposed method are 100%. The mean improvement of AR success rate is approximately 19.4% when fixing the fifth signal. Third, the TTFF for the first four signals of the proposed method is 1.00 s, which is significantly shorter than the one of the traditional method. For the fifth signal, approximately 49 s of TTFF can be shortened. In conclusion, the success rate and efficiency of AR can be significantly improved when using the proposed method.

In the future, the UD or DD multipath can also be parameterized in a similar way. Optimal multipath parameterization according to the user demands can be extended. Also, the proposed method can be used in other GNSS applications.

Acknowledgements This study is sponsored by the National Natural Science Foundation of China (42004014), the Natural Science Foundation of Jiangsu Province (BK20200530), the Fundamental Research Funds for the Central Universities (B210202109), China Postdoctoral Science Foundation (2020M671324), Jiangsu Planned Projects for Postdoctoral Research Funds (2020Z412), Science and Technology Innovation Project for Overseas Students in Nanjing. The authors are grateful for the comments from anonymous reviewers, which improved the quality of the paper.

Data availability The observation data of this study are available from the corresponding author for academic purposes on reasonable request.

References

Bock Y, Nikolaidis R, Jonge P, Bevis M (2000) Instantaneous geodetic positioning at medium distances with the global positioning system. J Geophys Res Solid Earth 105(B12):28223–28253

Cai C, He C, Santerre R et al (2016) A comparative analysis of measurement noise and multipath for four constellations: GPS, BeiDou, GLONASS and Galileo. Surv Rev 48:287–295

Chen D, Ye S, Xia J, Liu Y, Xia P (2016) A geometry-free and ionosphere-free multipath mitigation method for BDS three-frequency ambiguity resolution. J Geod 90(8):703–714

Cocard M, Bourgon S, Kamali O, Collins P (2008) A systematic investigation of optimal carrier-phase combinations for modernized triple-frequency GPS. J Geod 82(9):555–564

Daneshmand S, Broumandan A, Sokhandan N, Lachapelle G (2013) GNSS multipath mitigation with a moving antenna array. IEEE Trans Aerosp Electron Syst 49(1):693–698

de Bakker P, Tiberius C, van der Marel H, van Bree R (2012) Short and zero baseline analysis of GPS L1 C/A, L5Q, GIOVE E1B, and E5aQ signals. GPS Solut 16:53–64

Dong D, Bock Y (1989) Global positioning system network analysis with phase ambiguity resolution applied to crustal deformation studies in California. J Geophys Res Solid Earth 94(B4):3949–3966

Dong D, Wang M, Chen W, Zeng Z, Song L, Zhang Q, Cai M, Cheng Y, Lv J (2016) Mitigation of multipath effect in GNSS short baseline positioning by the multipath hemispherical map. J Geod 90(3):255–262

Feng Y (2008) GNSS three carrier ambiguity resolution using ionosphere-reduced virtual signals. J Geod 82(12):847–862

Forssell B, Martin-Neira M, Harris R (1997) Carrier phase ambiguity resolution in GNSS-2. In: Proceedings of ION GPS 1997, Kansas City, pp 1727–1736

Fuhrmann T, Luo X, Knöpfler A, Mayer M (2015) Generating statistically robust multipath stacking maps using congruent cells. GPS Solut 19(1):83–92

Henkel P, Iafrancesco M, Sperl A (2016) Precise point positioning with code multipath estimation. In: 2016 IEEE/ION Position, Location and Navigation Symposium-PLANS 2016

Lau L, Cross P (2007) Development and testing of a new ray-tracing approach to GNSS carrier-phase multipath modelling. J Geod 81(11):713–732
Leick A, Rapoport L, Tatarnikov D (2015) GPS satellite surveying. John Wiley & Sons, Hoboken
Li B (2018) Review of triple-frequency GNSS: ambiguity resolution, benefits and challenges. J Glob Pos Syst 16:1
Li B, Feng Y, Shen Y (2010) Three carrier ambiguity resolution: distance-independent performance demonstrated using semi-generated triple frequency GPS signals. GPS Solut 14(2):177–184
Li B, Zhang Z, Shen Y, Yang L (2018) A procedure for the significance testing of unmodeled errors in GNSS observations. J Geod 92(10):1171–1186
Li J, Yang Y, He H, Guo H (2020) Benefits of BDS-3 B1C/B1I/B2a triple-frequency signals on precise positioning and ambiguity resolution. GPS Solut 24:4
Lima Filho V, Moraes A (2020) Modeling multi-frequency GPS multipath fading in land vehicle environments. GPS Solut 25(1):3
Luo X, Mayer M, Heck B, Awange J (2014) A realistic and easy-to-implement weighting model for GPS phase observations. IEEE Trans Geosci Remote Sens 52(10):6110–6118
McGraw G, Braasch M (1999) GNSS multipath mitigation using gated and high resolution correlator concepts. In: Proceedings of the 1999 national technical meeting of the institute of navigation. pp 333–342
Moore M, Watson C, King M, Mcclusky S, Tregoning P (2014) Empirical modelling of site-specific errors in continuous GPS data. J Geod 88(9):887–900
Moradi R, Schuster W, Feng S, Jokinen A, Ochieng W (2015) The carrier-multipath observable: a new carrier-phase multipath mitigation technique. GPS Solut 19(1):73–82
Phan Q, Tan S, Mcloughlin I (2013) GPS multipath mitigation: a non-linear regression approach. GPS Solut 17(3):371–380
Pugliano G, Robustelli U, Rossi F, Santamaria R (2016) A new method for specular and diffuse pseudorange multipath error extraction using wavelet analysis. GPS Solut 20(3):499–508
Ragheb A, Clarke P, Edwards S (2007) GPS sidereal filtering: coordinate- and carrier-phase-level strategies. J Geod 81(5):325–335
Tang W, Deng C, Shi C, Liu J (2014) Triple-frequency carrier ambiguity resolution for Beidou navigation satellite system. GPS Solut 18(3):335–344
Teunissen P (1995) The least-squares ambiguity decorrelation adjustment: a method for fast GPS integer ambiguity estimation. J Geod 70(1–2):65–82
Teunissen P (1998) Success probability of integer GPS ambiguity rounding and bootstrapping. J Geod 72(10):606–612
Teunissen P, Joosten P, Tiberius C (2002) A comparison of TCAR, CIR and LAMBDA GNSS ambiguity resolution. In: Proceedings of ION GPS 2002, Portland, pp. 2799–2808
Teunissen P (1993) Least squares estimation of integer GPS ambiguities. In: Proceedings of section IV "Theory and Methodology," Beijing
Vollath U, Birnbach S, Landau L, Fraile-Ordoñez J, Martí-Neira M (1998) Analysis of three-carrier ambiguity resolution technique for precise relative positioning in GNSS-2. Navigation 46(1):13–23
Wang K, Rothacher M (2013) Ambiguity resolution for triple-frequency geometry-free and ionosphere-free combination tested with real data. J Geod 87(6):539–553
Wang K, Khodabandeh A, Teunissen P (2018) Five-frequency Galileo long-baseline ambiguity resolution with multipath mitigation. GPS Solut 22(3):75
Yang R, Xu D, Morton Y (2020) Generalized multi-frequency GPS carrier tracking architecture: design and performance analysis. IEEE Trans Aerosp Electron Syst 56(4):2548–2563
Ye S, Chen D, Liu Y, Jiang P, Tang W, Xia P (2015) Carrier phase multipath mitigation for BeiDou navigation satellite system. GPS Solut 19(4):545–557
Zhang X, He X (2016) Performance analysis of triple-frequency ambiguity resolution with BeiDou observations. GPS Solut 20(2):269–281
Zhang Z, Li B (2020) Unmodeled error mitigation for single-frequency multi-GNSS precise positioning based on multi-epoch partial parameterization. Meas Sci Technol 31(2):025008
Zhang Z, Li B, Gao Y, Shen Y (2019) Real-time carrier phase multipath detection based on dual-frequency C/N0 data. GPS Solut 23(1):7
Zhang Z, Li B, He X, Zhang Z, Miao W (2020) Models, methods and assessment of four-frequency carrier ambiguity resolution for BeiDou-3 observations. GPS Solut 24:96
Zhao Q, Dai Z, Hu Z, Sun B, Shi C, Liu J (2015) Three-carrier ambiguity resolution using the modified TCAR method. GPS Solut 19(4):589–599
Zheng D, Zhong P, Ding X, Chen W (2005) Filtering GPS time-series using a Vondrak filter and cross-validation. J Geod 79(6):363–369
Zheng K, Zhang X, Li P, Li X, Ge M, Guo F, Sang J, Schuh H (2019) Multipath extraction and mitigation for high-rate multi-GNSS precise point positioning. J Geod 93(10):2037–2051
Zhong P, Ding X, Yuan L, Xu Y, Kwok K, Chen Y (2010) Sidereal filtering based on single differences for mitigating GPS multipath effects on short baselines. J Geod 84(2):145–158

Zhetao Zhang obtained his Ph.D. with distinction from Tongji University, where his research topic was the GNSS unmodeled error. He is a researcher at the Hohai University and the Hong Kong Polytechnic University. His current research focuses on the GNSS precise positioning under complex conditions including canyon environment, low-cost receiver, and multi-GNSS situation. He was a research assistant and visiting Ph.D. student at the Hong Kong Polytechnic University and the University of Calgary, respectively.